# Chapter 6

# Method Development

In this section we present two alternative approaches for Green's function estimation using the data from two different stations. The first method uses the transfer function between the two sets of seismic information rather than the cross-correlation. The second method employs cepstral averaging to exploit the wavefield recorded at single station.

## 6.1 Transfer Function Approach

We have seen in §4.4 the important role that is played by secondary noise fields induced by seismic scattering in correlation methods. We will see that there is similar benefit when the transfer function between stations is considered.

We motivate the discussion by using the concept of local excitation at $\mathbf{x}_1$ and $\mathbf{x}_2$, recognizing that this is an oversimplification.

Consider local excitation $f(\mathbf{x}_1)$ at $\mathbf{x}_1$ recorded at $\mathbf{x}_2$. The ground velocity $v_f(\mathbf{x}_2, t)$ induced by the forcing can be represented in the convolutional form

$$v_{f1}(\mathbf{x}_2, t) = \int \mathrm{d}\tau\, H(\mathbf{x}_1, \mathbf{x}_2, t-\tau) f(\mathbf{x}_1, \tau), \tag{6.1}$$

where $H(\mathbf{x}_1, \mathbf{x}_2, t-\tau)$ is the appropriate Green's tensor element or its derivative [see, e.g., Kennett (2001)]. The forcing acts at the neighborhood of site $\mathbf{x}_1$, so we can represent the local velocity field as

$$v_1(\mathbf{x}_1, t) = v_f(\mathbf{x}_1, t) + w_1(\mathbf{x}_1, t) = Cf(\mathbf{x}_1, t) + w_1(\mathbf{x}_1, t), \tag{6.2}$$

where $w_1$ represents all other influences on ground motion. The actual velocity field at $\mathbf{x}_2$ will contain additional contributions so that

$$v_2(\mathbf{x}_2, t) = v_{f1}(\mathbf{x}_2, t) + w_2(\mathbf{x}_2, t), \tag{6.3}$$

where the coherence between $v_{f1}$ and $w_2$ can be expected to be small. The broad scale nature of the seismic noise field will mean that there will undoubtedly be some correlation.

If we now take the cross-correlation $\Phi_{12}$, then the spectrum will be

$$\begin{aligned}\bar{v}_1^*(\mathbf{x}_1,\omega)\bar{v}_2(\mathbf{x}_2,\omega) &= \bar{v}_{f1}(\mathbf{x}_2,\omega)\bar{v}_f^*(\mathbf{x}_1,\omega) + \bar{v}_{f1}(\mathbf{x}_2,\omega)\bar{w}_1^*(\omega) \\ &\quad + \bar{v}_f^*(\mathbf{x}_1,\omega)\bar{w}_2(\omega) + \bar{w}_2(\omega)\bar{w}_1^*(\omega).\end{aligned} \tag{6.4}$$

If we now take many independent estimates of the cross-correlation for separate time windows and average, then

$$\begin{aligned}\langle\bar{v}_1^*(\mathbf{x}_1,\omega)\bar{v}_2(\mathbf{x}_2,\omega)\rangle &\to \bar{v}_{f1}(\mathbf{x}_2,\omega)\bar{v}_f^*(\mathbf{x}_1,\omega) \\ &= \bar{H}(\mathbf{x}_1,\mathbf{x}_2,\omega)C|f(\mathbf{x}_1,\omega)|^2\end{aligned} \tag{6.5}$$

since the non-coherent parts will tend to cancel. This result demonstrates how the Green's function emerges from stacked cross-correlation measurements, but inevitably modulated by the power spectrum of excitation.

Now consider the transfer function between the recorded velocity field at $\mathbf{x}_1$ and $\mathbf{x}_2$: in the frequency domain

$$\begin{aligned}\frac{\bar{v}_2(\mathbf{x}_2,\omega)}{\bar{v}_1(\mathbf{x}_1,\omega)} &= \frac{\bar{v}_{f1}(\mathbf{x}_2,\omega)+\bar{w}_2(\omega)}{\bar{v}_f(\mathbf{x}_1,\omega)+\bar{w}_1(\omega)} \\ &= [\bar{v}_{f1}(\mathbf{x}_2,\omega)+\bar{w}_2(\omega)][\bar{v}_f^*(\mathbf{x}_1,\omega)+\bar{w}_1^*(\omega)] \\ &\quad \times\frac{1}{|\bar{v}_f(\mathbf{x}_1,\omega)+\bar{w}_1(\omega)|^2}\end{aligned} \tag{6.6}$$

so that the numerator has the same form as in (6.4). Taking again an ensemble average over many different time windows

$$\left\langle\frac{\bar{v}_2(\mathbf{x}_2,\omega)}{\bar{v}_1(\mathbf{x}_1,\omega)}\right\rangle \to \bar{H}(\mathbf{x}_1,\mathbf{x}_2,\omega)C\frac{|f(\mathbf{x}_1,\omega)|^2}{|f(\mathbf{x}_1,\omega)|^2+N(\omega)}. \tag{6.7}$$

We recall that we expect little coherence between $v_f(\mathbf{x}_1,t)$ and $w_1$ at any time, so that the bias term $N(\omega)$ will be small compared with $|f|^2$.

The averaged transfer function can thus be expected to give the correct phase behaviour for the Green's function between $\mathbf{x}_1$ and $\mathbf{x}_2$, but a slightly distorted amplitude spectrum. Interestingly, the presence of the bias term $N(\omega)$ is generally sufficient to ensure computational stability of the average transfer function. However, in practice, it is safer to use a water-level method (Helmberger & Wiggins, 1971) to avoid complications in the individual spectral divisions.

The averaged transfer function can be regarded as the deconvolution of the ground velocity field at $\mathbf{x}_2$ by that at $\mathbf{x}_1$. Unlike the cross-correlation there will be some directional character to estimates depending on the order in which the stations are selected. But, from seismic reciprocity both $\langle v_1(\omega)/v_2(\omega)\rangle$, $\langle v_2(\omega)/v_1(\omega)\rangle$ will provide estimates for the same Green's function. The simple derivation shows that the time averaged transfer function provides the same phase information but a broader frequency response than the averaged cross-correlation.

The analysis can be extended to include indirect excitation via stochastic noise field with the same result. Indeed the averaging provided by secondary scattering sources helps to improve the stability of the Green's function estimate.

### 6.1.1 Application to TASMAL Array

We demonstrate the effectiveness of the transfer function approach with results from the TASMAL experiment in Australia.

The conventional cross-correlation results are displayed in figure 6.1a, in the form of a record section so that the progression of the Rayleigh wave contribution can be clearly seen. We display the correlations with the records from station TL01, the northernmost station, so that interstation path lengths extend to 2000 km. from these vertical component records we extract a very clear set of fundamental mode Rayleigh wave arrivals, with some distinct variations in group velocity. The similar dominant frequency of the surface wave trains (around 0.125 Hz) can be directly associated with the main microseismic peak.

For comparison, the same set of noise records have been employed to generate the stacked transfer function between each station and TL01. The corresponding record section is shown in figure 6.1b, and we see immediately the much broader frequency content compared to the correlation results in figure 6.1a.

The closer stations to TL01 do not exhibit a fundamental difference between the cross-correlation and the transfer function results but the differences in areas with larger station separation. For stations TL12 and TL14, the retarded part of the Green's function due to south to north propagation is very weak in the cross-correlations; however, this low frequency propagation is recovered with the transfer function technique. We can attribute the higher frequency propagation from north to south as due to noise generation in the shallow continental shelf. In contrast to this, the deep waters of the Southern Ocean of the continent give rise to low frequency microseisms. Despite an improvement for the rest of the stations, the transfer function method failed to recover a satisfactory result for TL20; at the greatest range better estimates are likely with suitable pre-conditioning.

The arrival time difference for the Rayleigh waves at TL09 and TL10 is associated with the transition from Precambrian to Phanerozoic blocks of the continent. Although the interstation path for TL09 is greater than that for TL10, the arrival of Rayleigh wavetrains is earlier in the Precambrian region to the west. A similar situation occurs for the pairs TL07, TL08 and TL06, TL05, in each case the western station has earlier arrivals.

Similar results are obtained for all the other station combinations. As a result it is possible to significantly expand the frequency band over which group velocity measurements can be made and thereby significantly improve the available data for group velocity tomography across the region spanned by the TASMAL array.

The cross-correlations and transfer functions of station combinations in the east-west direction are given in figure 6.2. Similar to figure 6.1, the transfer function approach tends emphasize the low frequency propagation on the estimates.

The transfer function approach has the potential to enhance the low frequencies. By utilizing cross-correlation and transfer function estimates, the effective bandwidth can be increased, therefore the extent of the imaging between two stations.

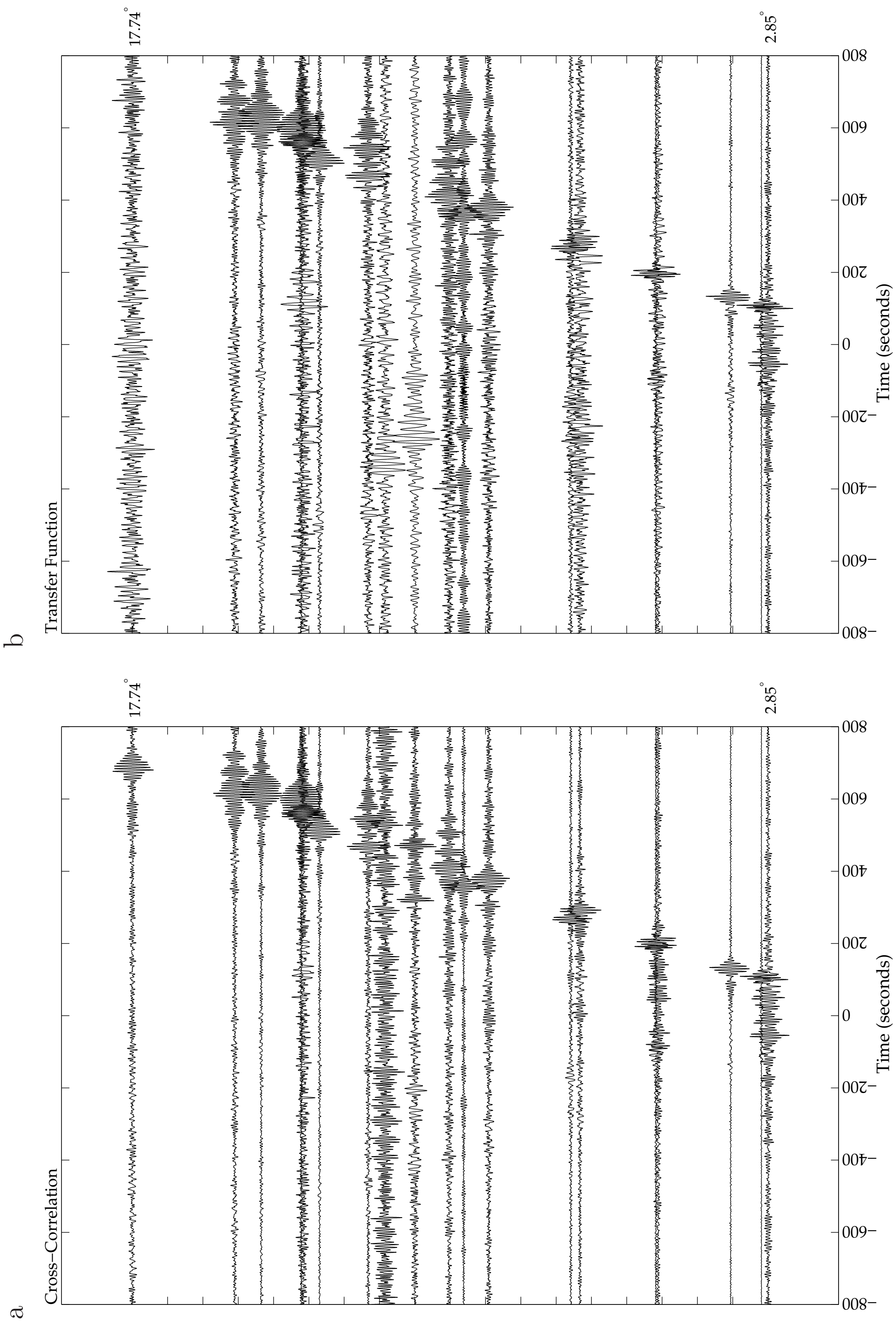


Figure 6.1: Unfiltered record section of stacked cross-correlation (a) and transfer functions (b) from station TL01 with an increasing interstation distance. Traces are normalized to the maximum amplitude.

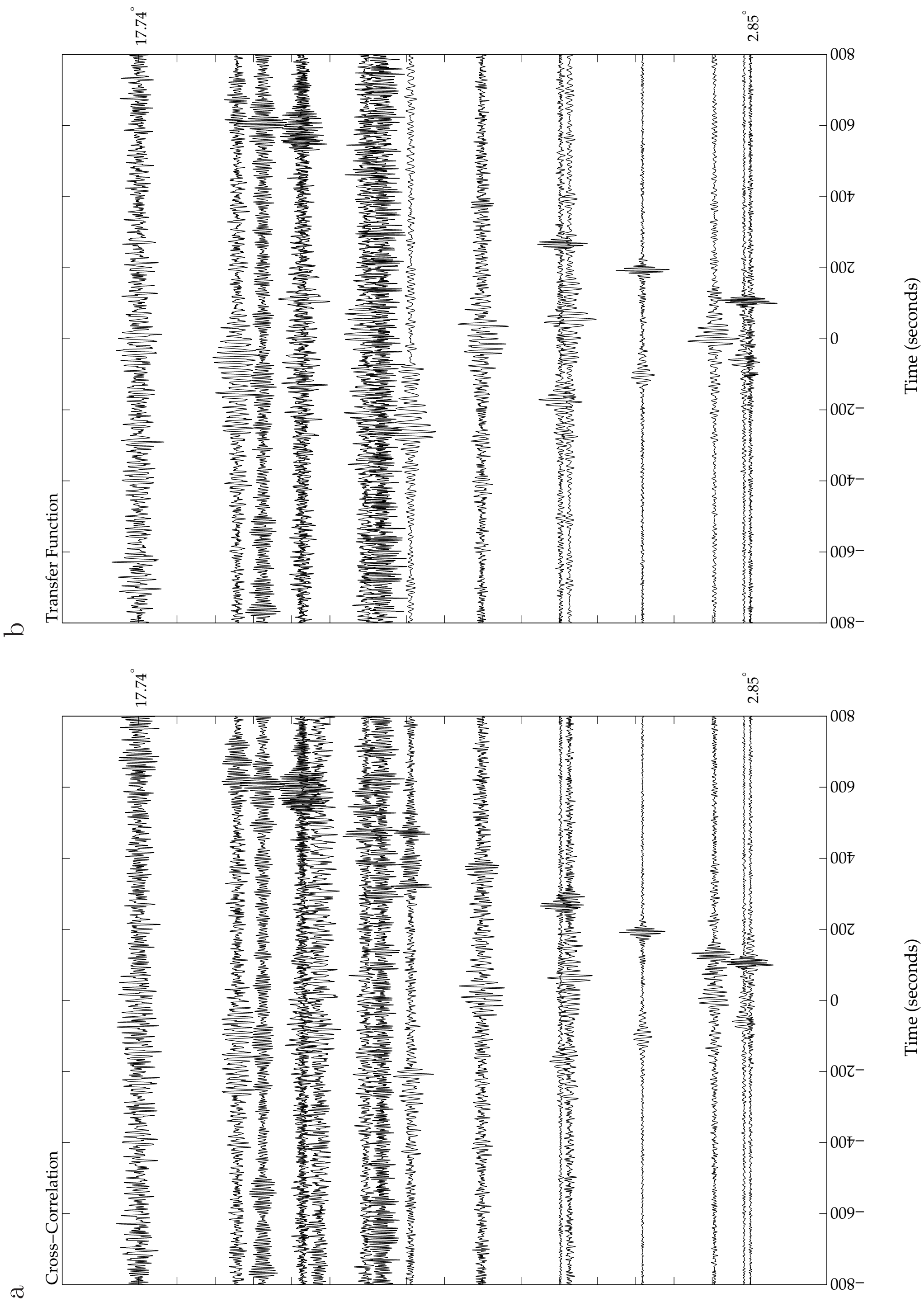


Figure 6.2: Unfiltered record section of stacked cross-correlation (a) and transfer functions (b) from station TL12 with an increasing interstation distance. Traces are normalized to the maximum amplitude.

## 6.2 Cepstral Averaging of Ambient Seismic Noise

The ambient noise which has random structure can be exploited by means of single station. With some assumptions, it can be shown that the recorded ambient noise at one station carries structural information which can be separated from the recorded signal. The fundamentals of the methodology and the results from real data application are presented.

### 6.2.1 Cepstrum Analysis

Oppenheim et al. (1968); Oppenheim (1969) proposed a class of nonlinear system which satisfies the general properties of superposition. The essential idea of homomorphic system theory was that many signal processing operations satisfy the same algebraic postulates as addition (Oppenheim & Schafer, 2004). By exploiting this property, a convolutional system can linearly be mapped into a system where the elements have the relation of addition.

If we consider a stable sequence $x(t)$, then its $z$-transform can be represented in polar form as

$$X(z) = |X(z)|\mathrm{e}^{\mathrm{i}\phi(z)}, \tag{6.8}$$

where $|X(z)|$ is the magnitude and $\phi(z)$ is the phase angle.

The complex natural logarithm of the $z$-transform is

$$\hat{X}(z) = \log[X(z)] = \log[|X(z)|\mathrm{e}^{\mathrm{i}\phi(z)}] = \log[|X(z)|] + \mathrm{i}\phi(z). \tag{6.9}$$

If we assume that the region of convergence for $X(z)$ includes the unit circle $z = \mathrm{e}^{\mathrm{i}\omega}$, then Fourier transformation can be defined for the above relations. In this case, the complex cepstra $\hat{x}(t)$ can be defined as the inverse Fourier transformation of the complex logarithm of the spectrum,

$$\hat{x}(t) = \frac{1}{2\pi}\int_{-\pi}^{\pi} d\omega \log[X(\omega)]\mathrm{e}^{\mathrm{i}\omega t}. \tag{6.10}$$

Although the name *complex cepstra* is given to the corresponding term, it does not have to be complex valued. For a real, stable sequence $x(t)$, the complex logarithm of the its spectra would be

$$\hat{X}(\omega) = \log[|X(\omega)|] + \mathrm{i}\arg[X(\omega)]. \tag{6.11}$$

The term $\log[|X(\omega)|]$ would always be a positive and even function of $\omega$, the phase term $\arg[X(\omega)]$ is an odd function of $\omega$, then the combination of these terms would have Hermitian symmetry in the frequency $\omega$ domain and the result of inverse Fourier transform $\hat{x}(t)$ would be real valued.

In traditional deconvolution, the operations are carried in frequency domain to use the multiplicative property of the frequency response of the system. For example by using different components as in receiver function analysis, one operator can be removed from the other by division. The homomorphic system concept which translates the convolutional properties of a system into addition can be used as a means of deconvolution. The characteristic function of a homomorphic system for convolution can be shown with $D_*$ which will map the convolution into addition, then addition to addition. We can show this relation for signals $x_1(t)$, $x_2(t)$ and their convolutional product $y(t)$,

$$D_*[y(t)] = D_*[x_1(t) * x_2(t)] = \hat{y}(t) = \hat{x}_1(t) + \hat{x}_2(t), \tag{6.12}$$

where the hat denotes the complex cepstras of the signals and $*$ is the convolution operator.

The seismic wavefield which is recorded mostly at the surface of the Earth is a result of series of effects. The general model which is accepted to describe these effects is convolutional model. According to this, the convolution of source wavelet, the reflections and transmissions at Earth's layered medium due to source and the instrument response creates the recorded signal at the receiver. By isolating one or other, one can exploit the part which is interested. In active and passive seismology studies, various isolation (deconvolution) methods are introduced to exploit the inherent information in the recorded signal.

The homomorphic system concept can be applied in order to deconvolve the seismic records. In the past, various studies showed for observational and theoretical data that is possible to utilize this technique (Butler, 1988; Li & Nábělek, 1999; Otis & Smith, 1977; Ulrych, 1971). However, the aim of this study is to show that rather than using a deterministic wavelet, e.g., earthquake signal, explosion, vibroseis, the noise field which is continuously acting in the Earth can be used for imaging beneath the station where the signal is recorded.

We consider a random excitation $f(\mathbf{x}, t)$ which is recorded at point $\mathbf{x}_1$ on the surface. By using the convolutional model we can represent the recorded velocity wavefield as

$$v(\mathbf{x}_1, t) = \int_{-\infty}^{\infty} d\tau H(\mathbf{x}_1, t - \tau) f(\mathbf{x}, \tau) + w(\mathbf{x}_1, t), \tag{6.13}$$

where $H(\mathbf{x}_1, t)$ is the impulse response beneath $\mathbf{x}_1$ and $w(\mathbf{x}_1, t)$ shows the other influences. If we rewrite the system in cepstral domain and ignore the effects of the other influences, then

$$\hat{v}(\mathbf{x}_1, t) = \hat{H}(\mathbf{x}_1, t) + \hat{f}(\mathbf{x}, t). \tag{6.14}$$

In eq.(6.14), the convolutional system of random excitation and the response of the Earth has been translated into addition. If the random excitation $f(\mathbf{x}, t)$ has a white spectrum, then in the log spectral domain, it will have a flat frequency distribution. Also if we assume that the response of the Earth has minimum phase characteristics and stationary in time, by introducing cepstral averaging we can unmix the recorded signal into its response and random excitation parts by enhancing the unchanging part of the signal (Earth's response) and suppressing the non-stationary part (random excitations). This can be shown as

$$\langle \hat{v}(\mathbf{x}_1, t) \rangle = \langle \hat{H}(\mathbf{x}_1, t) \rangle + \langle \hat{f}(\mathbf{x}, t) \rangle. \tag{6.15}$$

With sufficient stacking, we can expect to ignore $\langle \hat{f}(\mathbf{x}, t) \rangle$ compared to $\langle \hat{H}(\mathbf{x}_1, t) \rangle$ because of its variability. After cepstral averaging, by transforming back from cepstral domain into log-spectral domain, and then from log spectral domain into the time domain, the impulse response can be recovered;

$$\begin{aligned} \langle \hat{v}(\mathbf{x}_1, \omega) \rangle &= \int_{-\pi}^{\pi} dt [\langle \hat{v}(\mathbf{x}_1, t) \rangle] \mathrm{e}^{-\mathrm{i}\omega t} \\ &= \int_{-\pi}^{\pi} dt [\langle \hat{H}(\mathbf{x}_1, t) \rangle] \mathrm{e}^{-\mathrm{i}\omega t} \\ &= \hat{H}(\mathbf{x}_1, \omega), \end{aligned} \tag{6.16}$$

where

$$\widetilde{H}(\mathbf{x}_1, t) = \frac{1}{2\pi} \int_{-\pi}^{\pi} d\omega \exp[\hat{H}(\mathbf{x}_1, \omega)] \mathrm{e}^{\mathrm{i}\omega t} \tag{6.17}$$

represents the recovered impulse response due to the cepstral averaging.

To test this idea, daily seismic records from various broadband seismic experiments conducted in the Australian continent were used. The daily volumes have been divided into 3 hour segments for which the cepstras were calculated. This has been carried out for each of the days when the experiment was ran, then all of the cepstras were averaged for that particular station. By following the transformations shown in eq.(6.16) and eq.(6.17), the cepstras were converted into time domain. The output signals were bandpass filtered to enhance the final quality of the image.

The figures 6.3, 6.4, and 6.5, exhibit the frequency dependence of the recovered signal belonging to the same stations.

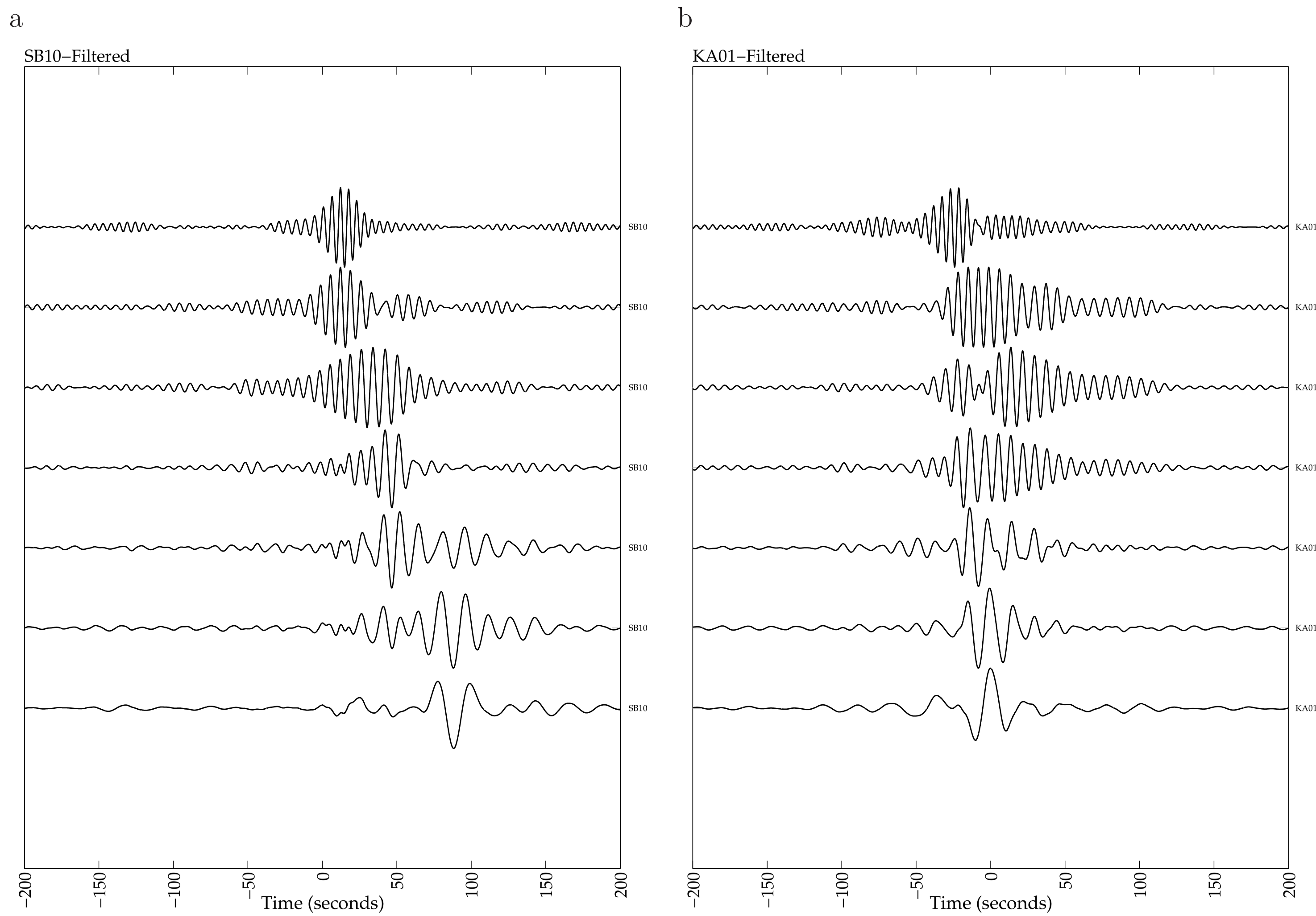


Figure 6.3: The effect of bandpass filtering on stations a) SB10 with stacking 39 cepstras. b) KA01 with stacking 49 cepstras. The frequencies from top to bottom trace are:0.16-0.2 Hz, 0.12-0.16 Hz, 0.1-0.14 Hz, 0.08-0.12 Hz, 0.06-0.1 Hz, 0.04-0.08 Hz, 0.02-0.05 Hz.

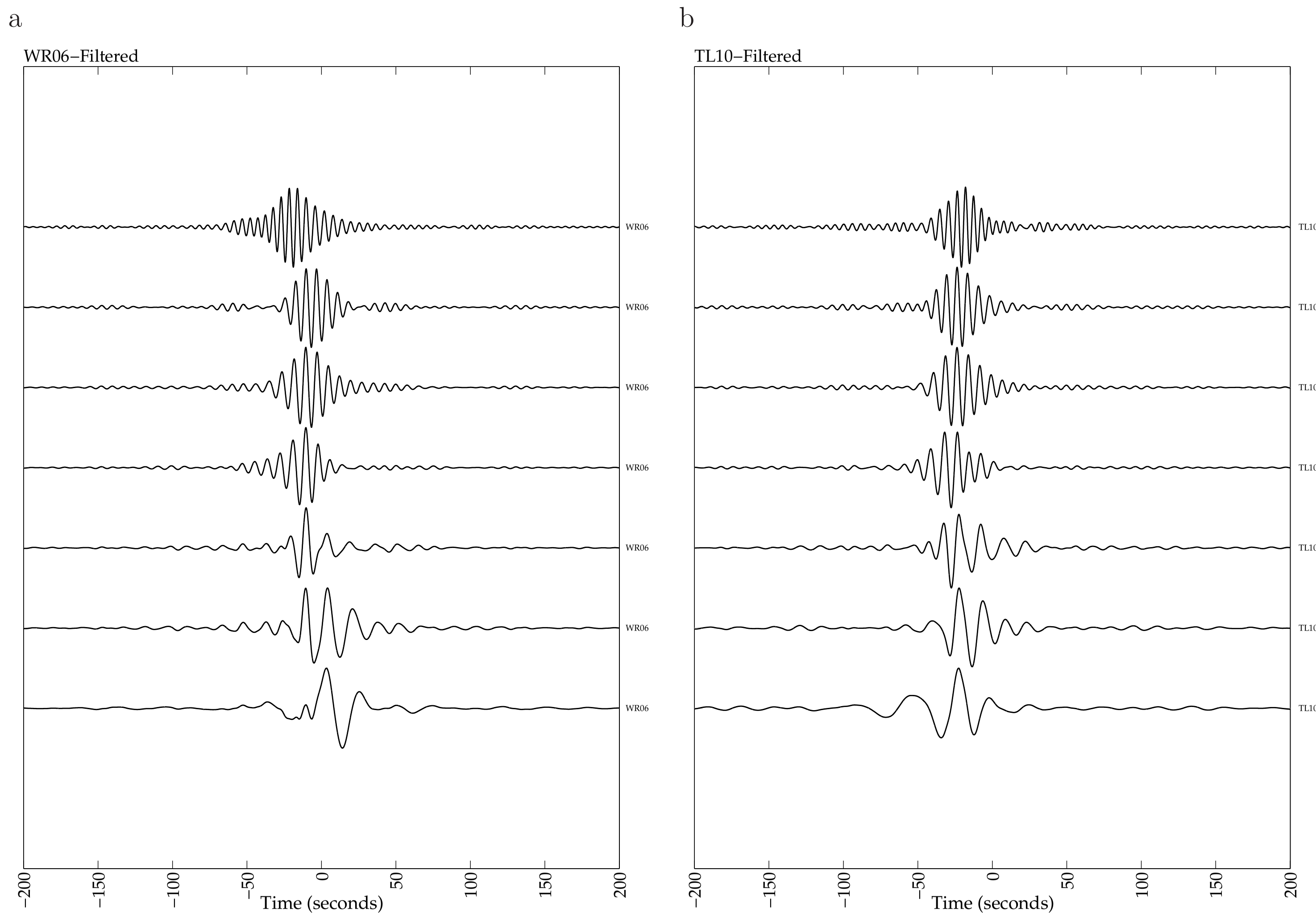


Figure 6.4: The effect of bandpass filtering on stations a) WR06 with stacking 32 cepstras. b) TL10 with stacking 35. The frequencies from top to bottom trace are:0.16-0.2 Hz, 0.12-0.16 Hz, 0.1-0.14 Hz, 0.08-0.12 Hz, 0.06-0.1 Hz, 0.04-0.08 Hz, 0.02-0.05 Hz.

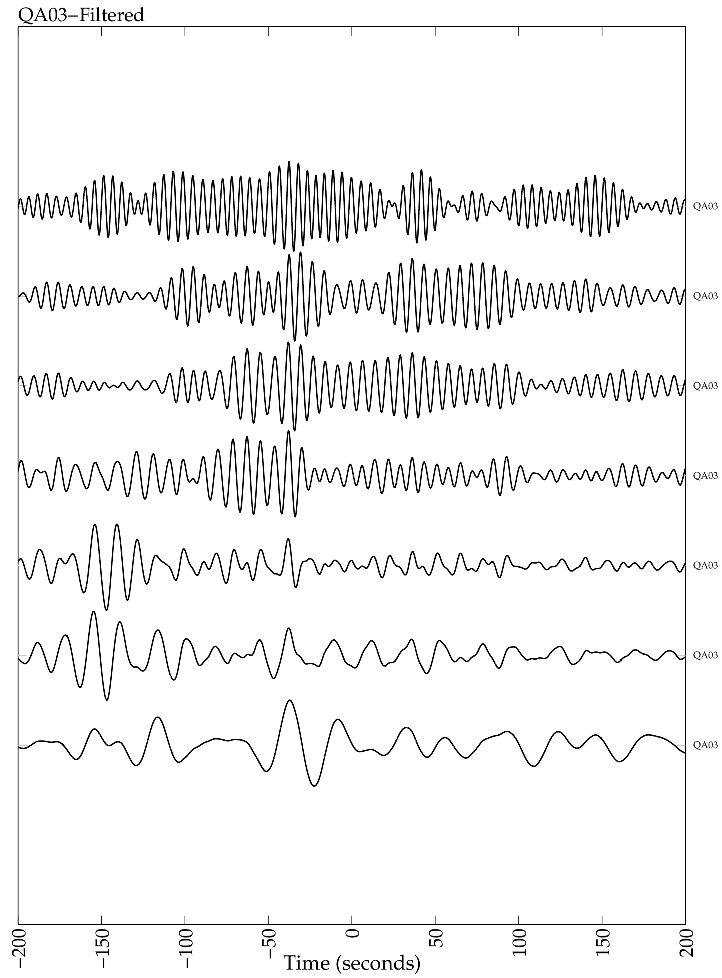


Figure 6.5: The effect of bandpass filtering on station QA03 with stacking 26 cepstras. The frequencies from top to bottom trace are:0.16-0.2 Hz, 0.12-0.16 Hz, 0.1-0.14 Hz, 0.08-0.12 Hz, 0.06-0.1 Hz, 0.04-0.08 Hz, 0.02-0.05 Hz.

### 6.2.2 Log Spectral Averaging

In the first section, the calculation was based on the averaging the complex cepstrum so that the separation of the noise field from the 1-D seismic response beneath the station might be achieved. In this part, the same idea is used but carried in a different way in order to see if there is a difference in the results due to the calculation scheme.

The seismic model dictates that the response of the Earth and the source wavelet has a convolutional relation. As we showed, Homomorphic system translates this relation into addition. The final product, the cepstrum was used for discriminating two fields. Rather than calculating the cepstrum, if the averaging is done in log spectral domain, can we get a better result?

If we use the same setup as the noise field $f(\mathbf{x}, t)$ at $\mathbf{x}$ is exciting the station at $\mathbf{x}_1$ we can represent the complex logarithms as

$$\begin{aligned}
\hat{v}(\mathbf{x}_1, \omega) &= \log[v(\mathbf{x}_1, \omega)] \qquad (6.18)\\
&= \log|v(\mathbf{x}_1, \omega)| + \mathrm{i}\arg v(\mathbf{x}_1, \omega)\\
&= \log|H(\mathbf{x}_1, \omega) f(\mathbf{x}, \omega)| + \mathrm{i}\arg\left[H(\mathbf{x}_1, \omega) f(\mathbf{x}, \omega)\right]\\
&= \log|H(\mathbf{x}_1, \omega)| + \log|f(\mathbf{x}, \omega)|\\
&\quad + \mathrm{i}\arg H(\mathbf{x}_1, \omega) + \mathrm{i}\arg f(\mathbf{x}, \omega),
\end{aligned}$$

where arg show the phase spectrum. The phase spectrum is a nonunique function which means that for same frequency bin, it can be multivalued. To carry the calculations, the phase should be unwrapped. A recent rooting algorithm for very high orders has been proposed by Sitton et al. (2003). By using this technique, the phase unwrapping was carried with high precision.

If we do the averaging in log spectral domain, then we can rewrite eq.(6.18) as

$$\begin{aligned}
\langle \hat{v}(\mathbf{x}_1, \omega)\rangle &= \langle \log|H(\mathbf{x}_1, \omega)|\rangle + \langle \log|f(\mathbf{x}, \omega)|\rangle \qquad (6.19)\\
&\quad + \langle \mathrm{i}\arg H(\mathbf{x}_1, \omega)\rangle + \langle \mathrm{i}\arg f(\mathbf{x}, \omega)\rangle.
\end{aligned}$$

Since the excitation field $f(\mathbf{x}, t)$ is random, we can expect that it will be suppressed with sufficient stacking. Then the relation in eq.(6.19) becomes

$$\langle \hat{v}(\mathbf{x}_1, \omega)\rangle \simeq \langle \log|H(\mathbf{x}_1, \omega)|\rangle + \langle \mathrm{i}\arg H(\mathbf{x}_1, \omega)\rangle. \qquad (6.20)$$

Then the time equivalent of the estimate can be written as

$$\widetilde{H}(\mathbf{x}_1, t) = \frac{1}{2\pi}\int_{-\pi}^{\pi} d\omega \exp[\acute{H}(\mathbf{x}_1, \omega)]\mathrm{e}^{\mathrm{i}\omega t}, \qquad (6.21)$$

where $\acute{H}(\mathbf{x}_1, \omega)$ is the averaged log spectrum of the Green's function in frequency domain.

In figure 6.6 and 6.7, an application on the SKIPPY array is given. In practice, the phase unwrapping algorithm relies on accurate root finding of $z$-transform of the input signal. With the given length of the signal, we had to downsample the signal from 25 Hz to 1 Hz to overcome the computational complexity of finding roots for very high degree polynomials. Each signal chosen for stacking had a duration of approximately 135 minutes. The stacking was done by choosing random segments with equal lengths from available continuous data ranging 20 to 69 days for each different station.

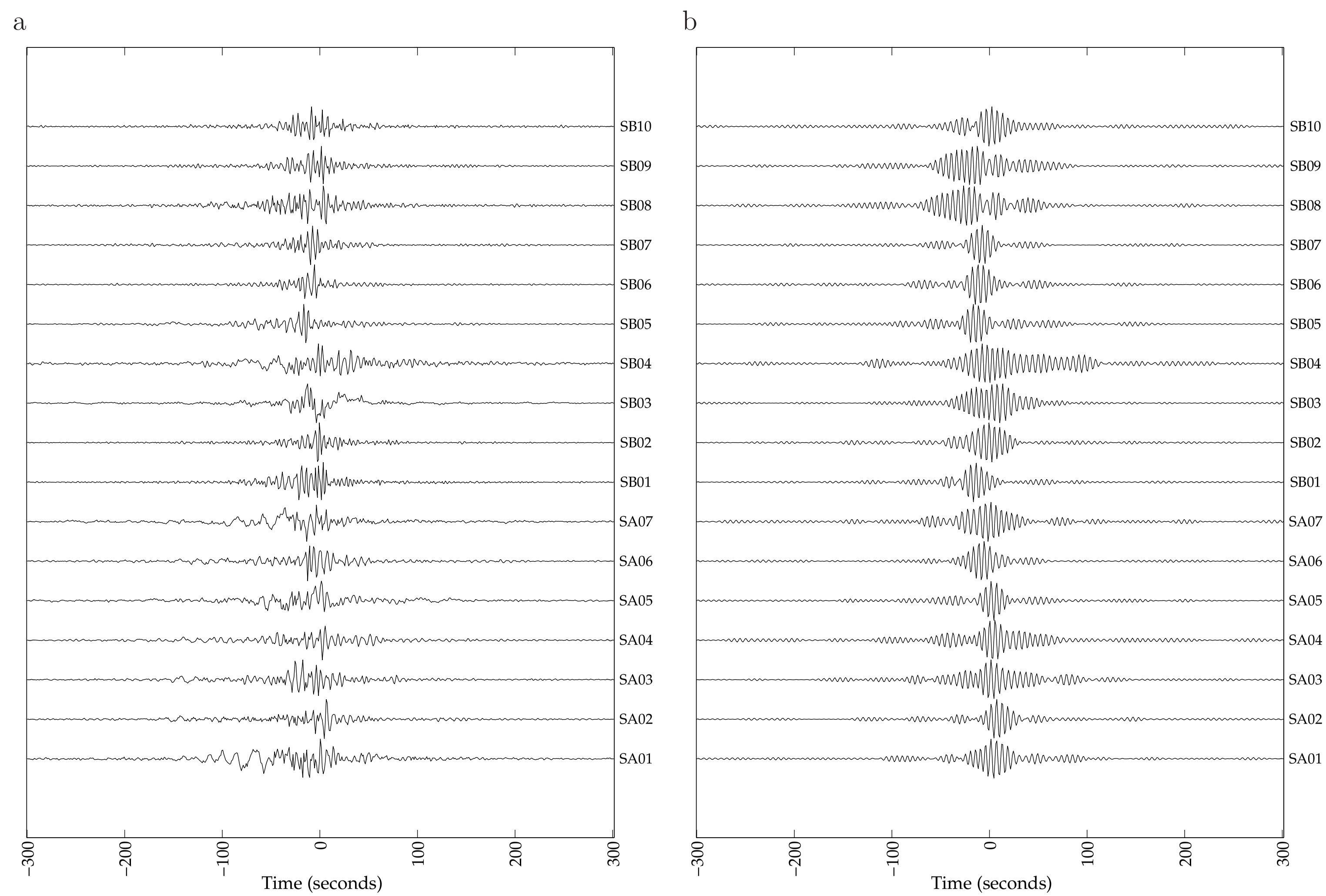


Figure 6.6: Log spectral averaging of SA and SB stations of SKIPPY experiment. a) Unfiltered sections. b) Bandpass filtered records with 0.16-0.2 Hz.

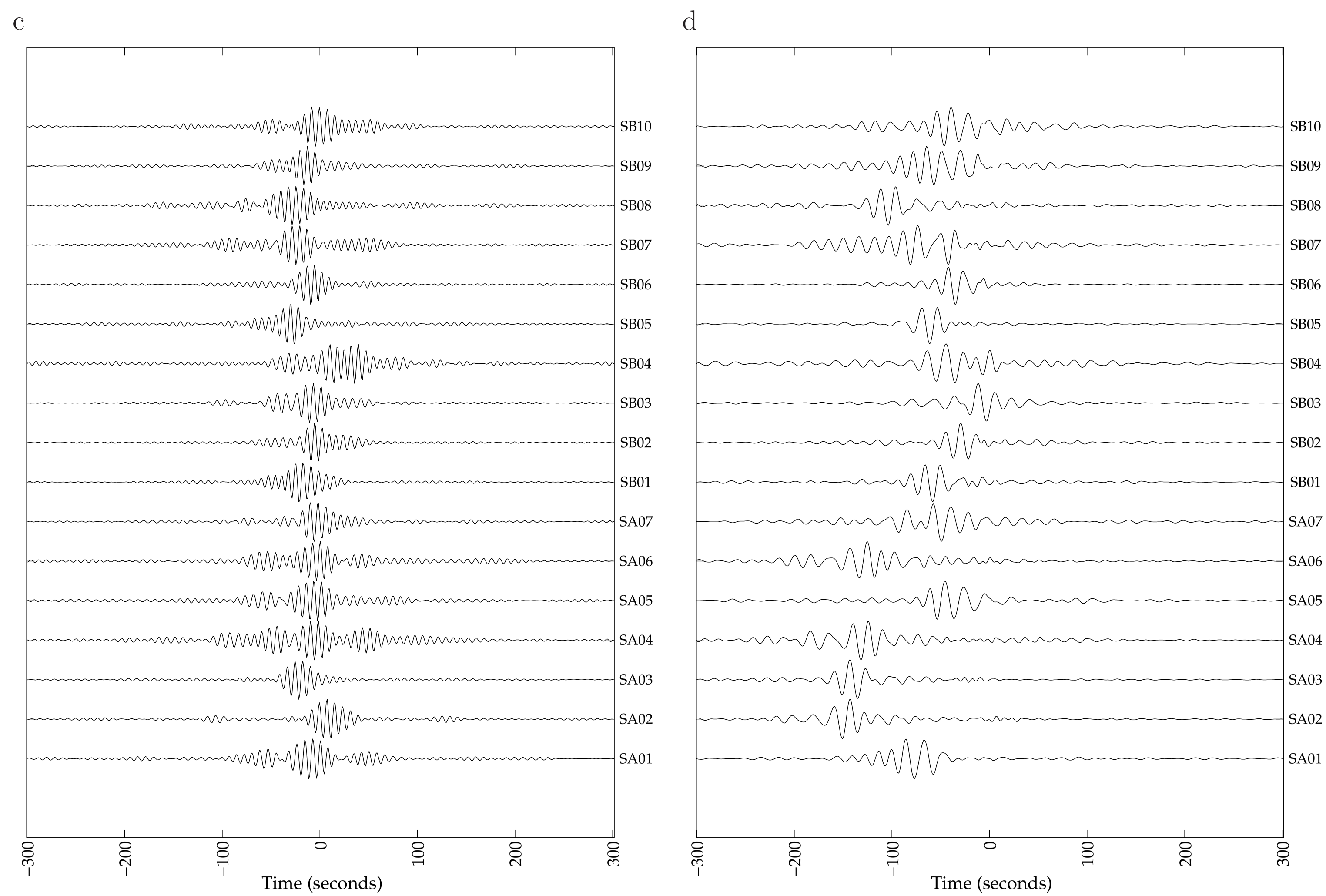


Figure 6.7: Log spectral averaging of SA and SB stations of SKIPPY experiment. a) Bandpass filtered records with 0.1-0.14 Hz. b) Bandpass filtered records with 0.04-0.08 Hz.

### 6.2.3 Interpretation of Local Responses

The contributions for each of the sites show clear dispersion in frequency and significant variation between locations. We can gain an insight into the nature of the local response by considering the potential excitation field. The 'noise-field' will be dominantly composed of fundamental model Rayleigh waves generated well away from the site, with secondary contributions from local scattering.

For high frequency surface waves, the asymptotic theory of Woodhouse (1974) shows that at each point along the propagation path, the properties of a surface wave depend on the layered structure and dispersion characteristics beneath that point. This local structure will be common to surface waves whatever their direction of propagation or distance from the source.

The fundamental mode contribution for a surface wave in a medium with weak lateral variations can be expressed as (Kennett, 1995)

$$\mathbf{u}(X, \phi, t) \approx \sum_m \mathrm{e}^{\mathrm{i}m\phi} \int_{-\infty}^{\infty} d\omega \mathrm{e}^{-\mathrm{i}\omega t} \mathcal{S}^m(p_0^s, \omega)\mathcal{R}(p_0^r, \omega)\mathcal{P}(X, \omega, \mathrm{path}), \quad (6.22)$$

where $X$ is the epicentral distance and $\phi$ is the azimuth from the source. The source excitation $\mathcal{S}^m(p_0^s)$ depends on the azimuthal order $m$, but the receiver term $\mathcal{R}(p_0^r)$ and the path contribution $\mathcal{P}(X, \mathrm{path})$ do not. The asymptotic properties demonstrated by Woodhouse (1974) are included in the dependence of the local phase slowness $p$ at source and receiver.

In the frequency domain, for an isotropic medium, we can write eq.(6.22) as

$$\mathbf{u}(X, \phi, \omega) \approx \mathcal{R}(p_0^r, \omega) \left\{ \sum_m \mathrm{e}^{\mathrm{i}m\phi} \mathcal{S}^m(p_0^s, \omega)\mathcal{P}(X, \omega, \mathrm{path}) \right\}, \quad (6.23)$$

and recognize that the receiver term is in common whatever the source character.

Under logarithmic transformation

$$\log \mathbf{u}(X, \phi, \omega) \approx \log \mathcal{R}(p_0^r, \omega) + \log \left\{ \sum_m \mathrm{e}^{\mathrm{i}m\phi} \mathcal{S}^m(p_0^s, \omega)\mathcal{P}(X, \omega, \mathrm{path}) \right\}. \quad (6.24)$$

The receiver term will be emphasized when stacking over many periods of noise excitation:

$$\langle \log \mathbf{u}(X, \phi, \omega) \rangle \approx \langle \log \mathcal{R}(p_0^r, \omega) \rangle. \quad (6.25)$$

If there is weak azimuthal anisotropy for the surface waves then there will be a directional dependence to $\mathcal{R}$, but averaging over many directions of incident noise is expected to extract the isotropic contribution.

The contribution $\mathcal{R}$ depended on the local structural properties through the eigenfunction of the fundamental Rayleigh mode. Lower frequency contributions will be influenced by deeper structure (cf. figure 6.6b and figure 6.7b). As a result there will be a significant frequency dependence to the local contribution extracted by stacking as in eq.(6.25).

The contributions illustrated in figure 6.6a thus contain information on the structure beneath each site, but the dependence is somewhat indirect. Further effort will be needed to work out how to exploit this new source of information.